

Investigation of Positive Feedback Anti-Islanding Control for Multiple Inverter-Based Distributed Generators

Xiaoyu Wang, *Member, IEEE*, Waldir Freitas, *Member, IEEE*, Venkata Dinavahi, *Member, IEEE*, and Wilsun Xu, *Fellow, IEEE*

Abstract—The positive feedback-based anti-islanding scheme has become a common anti-islanding protection technique for inverter-based distributed generators (DGs). This paper investigates the scheme's impact on the small-signal stability of multiple inverter-based DGs installed in power distribution systems during grid-connected operation. The interactions among multiple-DGs due to the anti-islanding scheme are also addressed. An index is proposed to quantify the destabilizing effect of the aggregated positive feedback activities of multiple DGs. This paper further introduces a DG power transfer limit versus islanding detection time curve to reveal the conflicting requirements of anti-islanding protection speed and the maximum power transfer of multi-DG systems.

Index Terms—Distributed generator, inverter, islanding, positive feedback, small-signal model.

I. INTRODUCTION

DISTRIBUTED generation (DG) has gained popularity in recent years. Providing protection against islanding is probably one of the most challenging issues to be addressed in DG applications. An island occurs when a portion of the distribution system becomes electrically isolated from the remainder of the power system, yet continues to be energized by distributed generators (DGs). The capability of a DG unit to detect if it operates in an islanded system and to disconnect itself from the system in a timely fashion is an important requirement for DGs [1].

In the case of inverter-based DGs, the positive feedback-based anti-islanding methods have gained wide acceptance. These methods use the deviations of voltage frequency and/or magnitude from normal values as positive feedback signals to influence the operation of inverter-based DGs [2]–[4]. The essential idea is to destabilize a DG when it is islanded, which facilitates the detection of islanding condition.

Since the positive feedback scheme is a destabilizing force, the impact of this scheme on the stability of a grid-connected

DG system and on other DGs becomes a natural concern when a large number of inverter-based DG is connected to a weak supply system. If the positive feedback gain is too high, the DG system may become unstable even if it is connected to the main supply system. In order to maintain stability level, the size and number of DGs connected to the system may have to be reduced. The destabilizing force produced by different inverters could also interact and affect the local stability of individual DG unit.

Reference [5] studied the DG-to-system stability issue for a single DG. The purpose of this paper is to present our research findings on the DG-to-system and DG-to-DG stability impacts when multiple DGs are installed. Based on the modal analysis approach [6], [7], the *multi-DG power transfer limit versus positive feedback gain curve* ($P - K$ curve) is proposed in this paper as a tool to quantify the impact of positive feedback on the system stability. Main factors affecting the small-signal stability of multi-DG systems are analyzed and discussed through an extensive sensitivity study. The conflict between the multi-DG stability and the islanding detection capability is also explored by using *DG power transfer limit versus islanding detection curve* ($P - t$ curve). The Sandia frequency shift (SFS) method is selected as a representative of these schemes.

This paper is organized as follows. Section II briefly introduces the principle of the positive feedback anti-islanding scheme. Section III discusses the power transfer limit of multiple DGs in distribution systems and the concept of $P - K$ curve is explained. In Section IV, the key factors affecting the multi-DG penetration limit are investigated by using this concept. The interactions among multiple DGs caused by the anti-islanding control are presented in Section V. Section VI presents the investigation results on DG islanding detection time. Section VII summarizes the conclusions. The multi-DG system small-signal model is included in Appendix A. The small signal model is validated in Appendix B by comparing the results obtained by this model with the results obtained by electromagnetic transient simulations using detailed, nonlinear models. Appendix C presents the system data.

II. PRINCIPLE OF POSITIVE FEEDBACK ANTI-ISLANDING SCHEME

The positive feedback scheme is a general concept that uses the deviations of voltage magnitude or frequency at the point of common coupling (PCC) from normal values as a positive feedback signal to influence the controller operation of the inverter-based generator. When the generator is operated in the grid-parallel mode, the voltage magnitude and frequency will

Manuscript received April 22, 2008; revised July 11, 2008. First version published December 09, 2008. Current version published April 22, 2009. This work was supported by Natural Resources Canada through the Technology and Innovation Program as part of the Climate Action Plan for Canada. Paper no. TPWRS-00323-2008.

X. Wang is with the Electrical Engineering Department, Tsinghua University, Beijing 100084, China (e-mail: xiaoyuw@ieee.org).

W. Freitas is with the Department of Electrical Energy Systems, University of Campinas, Campinas 13083-852, Brazil (e-mail: waldir@ieee.org).

V. Dinavahi and W. Xu are with the Department of Electrical and Computer Engineering, University of Alberta, Edmonton, AB T6G 2V4 Canada (e-mail: wangxy@ece.ualberta.ca; dinavahi@ece.ualberta.ca).

Digital Object Identifier 10.1109/TPWRS.2008.2007002

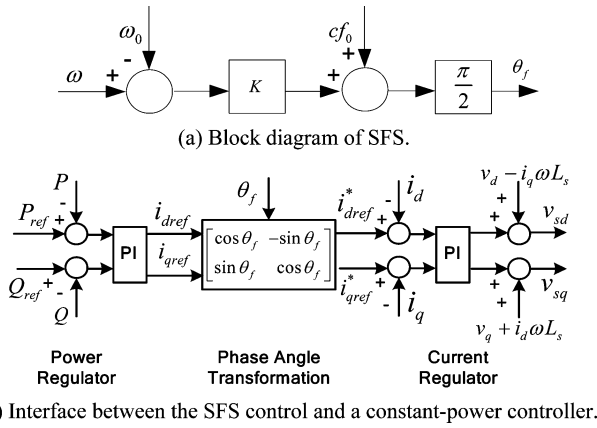
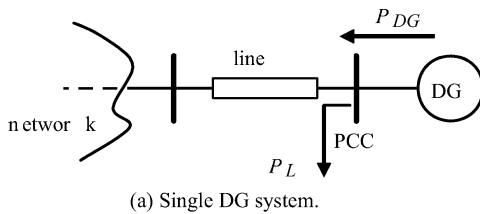
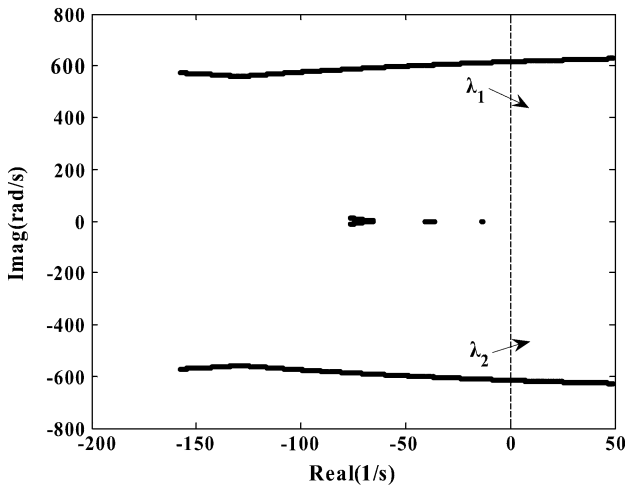


Fig. 1. Diagram block of the SFS and a constant-power controller.



(a) Single DG system.



(b) Root loci of all the eigenvalues for a single DG system.

Fig. 2. Small-signal stability for a single DG system.

be regulated by the network. As a result, the PCC voltage magnitude and frequency will be kept at the grid level in spite of the positive feedback. On the other hand, when the grid is lost the PCC voltage will be decided by the inverter controller. Due to the positive feedback, the voltage magnitude or frequency will drift from their nominal value and the islanding can be detected by under/over voltage or frequency relays.

The SFS method is a positive feedback anti-islanding method that uses the frequency bias of the PCC voltage as the feedback signal, as shown in Fig. 1. It is chosen as the representative positive feedback anti-islanding method to be studied in this paper. The details of the SFS method applied to single-phase generators can be found in [8] and its extension to three-phase generators is explained in [5], where the symbol notation is also described.

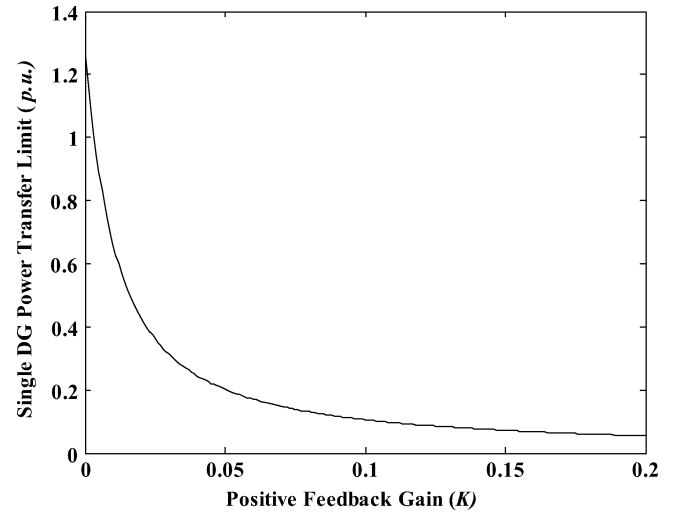


Fig. 3. Single DG P-K curve of the DG power transfer characteristic.

The positive feedback anti-islanding scheme is designed to destabilize the islanded DG system in the event of grid disconnection. On the other hand, it is assumed that the destabilizing force of the positive feedback control is comparatively small and has little impact on the DG stability when the DG is connected to the grid. This assumption may not be true if the DG penetration level is high. In order to clarify this concern, this paper conducts a sensitivity study on the small-signal stability of multiple inverter-based DGs with the positive feedback anti-islanding protection during grid-parallel connection.

III. MULTI-DG POWER TRANSFER LIMIT VERSUS POSITIVE FEEDBACK GAIN CURVE

The *multi-DG power transfer limit (P) versus positive feedback gain (K) curve* is proposed as a stability index in the study. Before introducing the power transfer limit versus positive feedback gain curve for a multi-DG system, it is important to understand such a concept for a single DG system. For the system shown in Fig. 2(a), there is a technical limit for the active power P_{DG} produced by the generator with the positive feedback anti-islanding protection because of small-signal stability restrictions. Fig. 2(b) shows the root loci of the single-DG system eigenvalues when the SFS positive feedback gain K is fixed at 0.03 and the active power produced by the DG is gradually increased from 0 p.u. to 0.5 p.u. The load power P_L is fixed. This figure shows that one pair of conjugate eigenvalues (λ_1 , λ_2) move from the left half-plane to the right half-plane when the DG power is increased. The critical eigenvalues λ_1 and λ_2 cross the imaginary axis when DG power is increased to 0.31 p.u., which is the DG power transfer limit for $K = 0.03$. Accordingly, for each value of the positive feedback gain, a value of DG power transfer limit can be obtained by the eigenvalue analysis. Fig. 3 displays how the power transfer limit changes with the change in K from 0 to 0.2. The $P-K$ curve shows that when the positive feedback gain is low, the DG can transfer more power to the grid, however, this limit is reduced when K increases. In addition, the $P-K$ curve reveals how the DG stability level changes due to the positive feedback anti-islanding control.

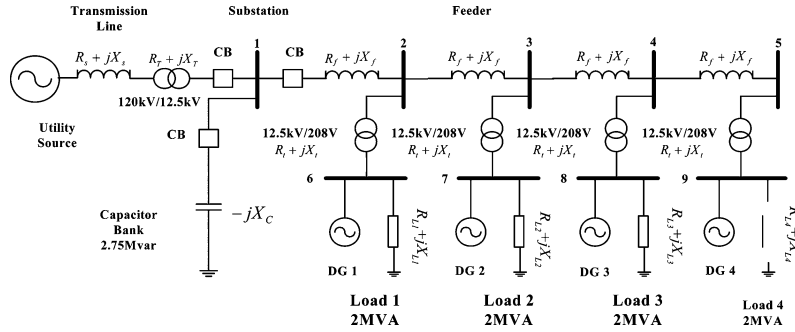


Fig. 4. Schematic diagram of the test distribution system feeder with multiple inverter-based DGs.

From Fig. 3, it is seen that a single DG power transfer limit can be related to the positive feedback gain of the DG anti-islanding control through the $P - K$ curve, expressed as

$$P_{\max} = f(K) \quad (1)$$

where the function of the curve is f ; P_{\max} is the power transfer limit from the DG to the network from stability viewpoint and K is the positive feedback gain. In multi-DG applications, a similar curve can be derived. The $P - K$ curve in the presence of multiple DGs can be expressed as

$$P_{\max} = f(K_1, K_2, \dots, K_n) \quad (2)$$

where the total multi-DG power transfer limit is P_{\max} , the positive feedback gains K_1, K_2, \dots, K_n , are related to the anti-islanding control of DG1, DG2, ..., DGn, respectively, and n is the number of DGs. It is important to note that the relationships between each positive feedback gain and the maximum power transfer limit of each generator are not independent in the function f because the multiple DGs interact with each other through the distribution network. The multi-DG $P - K$ curve can be obtained from the modal analysis approach based on the small-signal model presented in Appendix A of the paper, and it will be used for the sensitivity studies presented in the following section.

IV. FACTORS AFFECTING THE MULTI-DG PENETRATION LEVEL

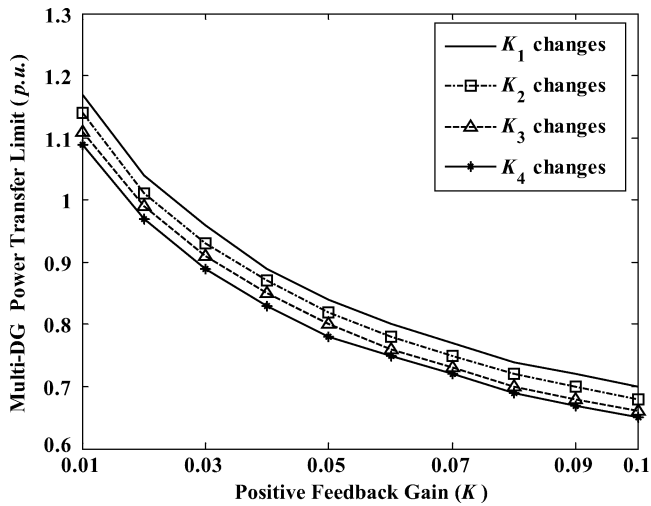
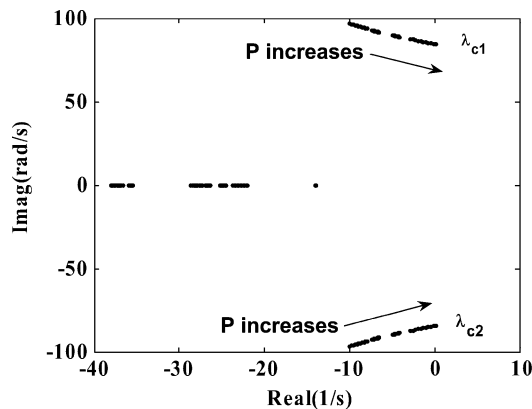
With the $P - K$ curve, the collective impact of the positive feedback anti-islanding control on the small-signal stability of multi-DG systems can be quantified and the factors affecting the penetration limit of multiple DGs for a distribution system can be investigated comparatively. This section presents the investigation results on several factors that affect the multi-DG penetration limit level. The main factors analyzed were DG location, number of DGs, substation capacitor size, transformer sizes, and feeder length. In order to carry out these stability studies, the Canadian urban benchmark distribution system proposed in [9] is utilized. The schematic diagram of the test system is shown in Fig. 4. The data of the system can be seen in Tables II and III in Appendix C. The utility source is 120 kV and the 12.5 kV substation is connected to the grid through a circuit breaker (CB) and a substation transformer with a capacity of 10 MVA. A 2.75 Mvar capacitor bank is located at the substation. Four inverter-based DGs (three-phase 208 V) are evenly distributed

along the feeder. They are connected to the feeder through the step-down transformers and the DG terminals are from Node 6 to Node 9 in sequence. The constant impedance load model with power factor 0.95 is adopted to represent the local load of each generator. The DGs are constant power-controlled and all of them are equipped with the SFS anti-islanding control.

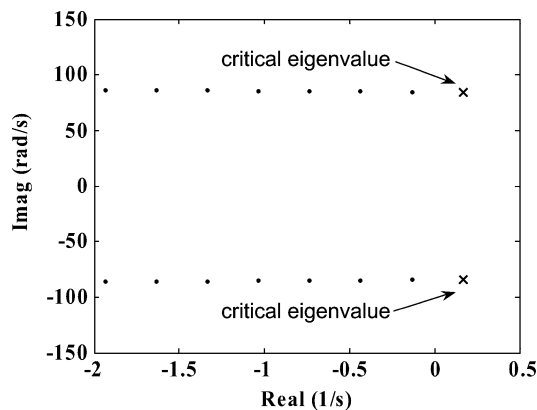
A. DG Location

As multiple DGs are installed along the distribution feeder, the distance from each DG to the substation is different. The impact of DG location on the multi-DG penetration limit is illustrated by Fig. 5, where four $P - K$ curves are shown. For “ K_1 changes” curve, the positive feedback gains of DG2, DG3, and DG4 (K_2, K_3, K_4) are set as zero and the DGs output powers (P_2, P_3, P_4) are fixed at 0.1 p.u. The positive feedback gain of DG1 (K_1) is increased to observe the changes in its output power limit (P_1). The total multi-DG penetration limit will be the sum of P_1, P_2, P_3 , and P_4 . The other three curves are obtained in the same way by fixing three DGs gains and output powers and varying the gain and power of the other DGs. One can see that the multi-DG power transfer limit is the highest for the “ K_1 changes” curve and the lowest for the “ K_4 changes” curve when the positive feedback gains of the four curves are the same. This means that DG1 in the former case can produce more power than DG4 in the later case. In other words, the DG near to the substation has less impact on the multi-DG small-signal stability than the DG far away from the substation.

This phenomenon can be further investigated and confirmed by analyzing the participation factor of the four DGs. Fig. 6(a) shows the root loci of the multiple DG system for the following situation: the four positive feedback gains are set as 0.1 and the active power of the four DGs is changed simultaneously and equally to get the root loci of the system eigenvalues. By this setting, the only difference among the DGs is the location. When the DGs output power is increased to some level, there will be a pair of critical eigenvalues ($\lambda_{c1}, \lambda_{c2}$) whose real parts become positive, which is shown in Fig. 6(b). The participation factors of the DGs’ state variables to the critical mode are displayed in Fig. 7, which reveals that DG4 variables have the highest magnitude of the participation factors and DG1 variables have the lowest one. This result indicates that DG4 is more prone to become unstable compared to the other DGs in the multiple DG system. An eigenvalue sensitivity study was also conducted based on the modal analysis of Fig. 6. The sensitivity of the critical eigenvalue λ_{c1} to the DG positive feedback gains is shown in Table I. The result shows that the critical eigenvalue is more

Fig. 5. Multi-DG $P - K$ curves for the multiple DGs.

(a) Root loci of the multiple DG system eigenvalues.



(b) Dislocation of the critical eigenvalues.

Fig. 6. Root loci of the multiple DG system eigenvalues.

sensitive to changes in K_4 , which means the positive feedback control of DG4 is more prone to become unstable.

The reason for the above observation is mainly due to the fact that when the DG is far away from the substation it has a relatively weak link with the power system, in this case represented by the utility source. As a result, this DG may lose its stability easier if there are unstable factors affecting it, such as the positive feedback anti-islanding control.

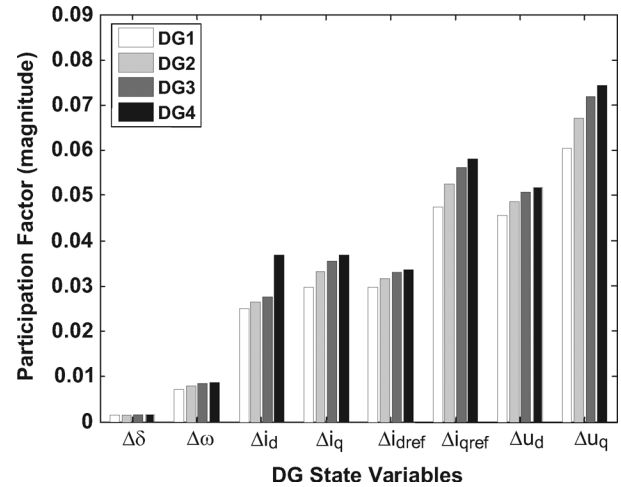


Fig. 7. Participation factors of multiple DGs.

TABLE I
CRITICAL EIGENVALUE SENSITIVITY ANALYSIS

| $ \partial\lambda_{c1}/\partial K_1 $ | $ \partial\lambda_{c1}/\partial K_2 $ | $ \partial\lambda_{c1}/\partial K_3 $ | $ \partial\lambda_{c1}/\partial K_4 $ |
|---------------------------------------|---------------------------------------|---------------------------------------|---------------------------------------|
| 8.4079 | 9.3147 | 9.9555 | 10.2871 |

B. DG Number

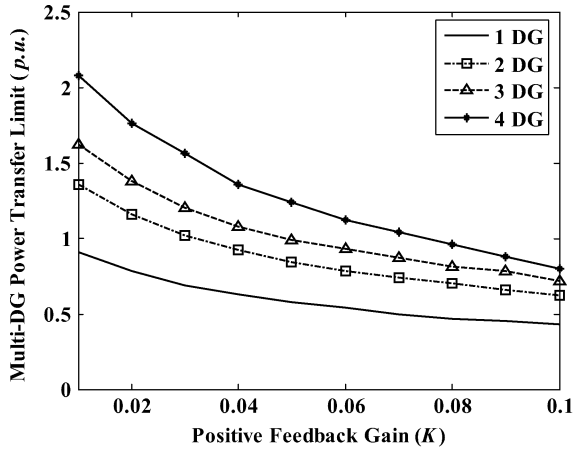
The impact of DG number on the test DG system penetration level is shown in Fig. 8, where the results for the following cases are presented:

- 1) "1 DG" case—Only DG1 is installed in the feeder;
- 2) "2 DG" case—Only DG1 and DG2 are installed, each DG has the same output power and positive feedback gain;
- 3) "3 DG" case—Only DG1, DG2 and DG3 are installed, each DG has the same output power and positive feedback gain;
- 4) "4 DG" case—All of the DGs are installed, each DG has the same output power and positive feedback gain.

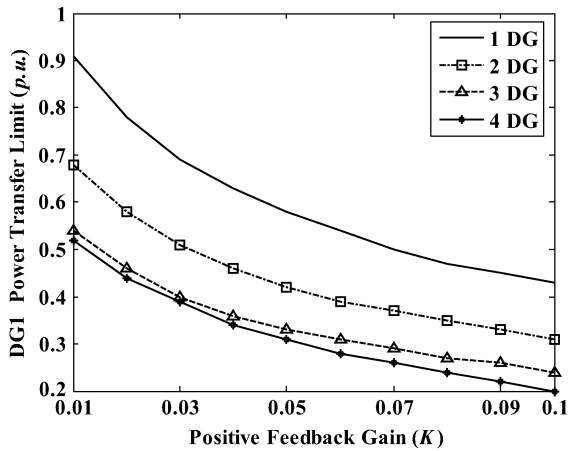
Fig. 8(a) displays the total multi-DG power transfer limit curves. From this figure, one can see that the total multi-DG power transfer increases when there are more DGs spread in the distribution system. However, the single DG power transfer limit is decreased with the increase in the DG numbers, which is exhibited in Fig. 8(b) where the limit of DG1 is shown. This is mainly due to the collective influence of the positive feedback anti-islanding control resident in multiple DGs. If the DG owners are different, the DG1 owner will be adversely affected by the presence of the other DGs since the power production has to be reduced.

C. Substation Capacitor

The capacitor bank installed at the substation provides reactive power to the distribution feeder. Fig. 9 illustrates the impact of the substation capacitor size on the multiple DG penetration limit from the small-signal stability viewpoint. These $P - K$ curves were determined considering that all DGs have the same output power and positive feedback gain. Each curve in Fig. 9 represents different capacity of the substation capacitor bank. This figure reveals that when the reactive compensation installed at the substation increases the multi-DG penetration level also increases. A large size of the substation capac-



(a) Multi-DG power transfer limit for different DG numbers.



(b) DG1 power transfer limit for different DG numbers.

Fig. 8. Impact of DG number on the multi- and single DG $P - K$ curve.

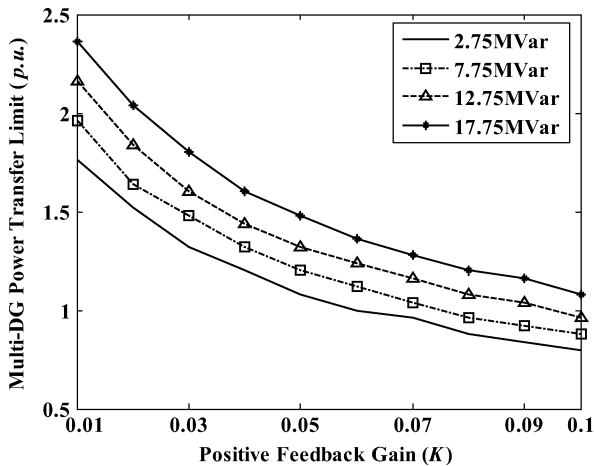
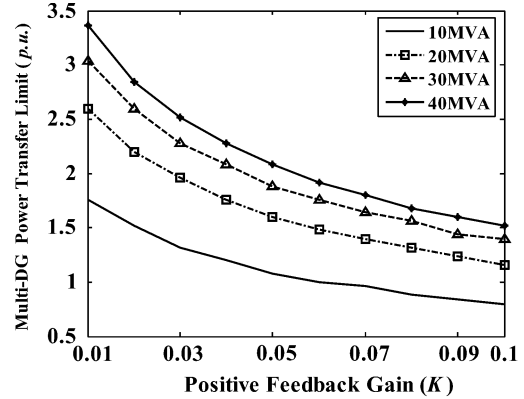
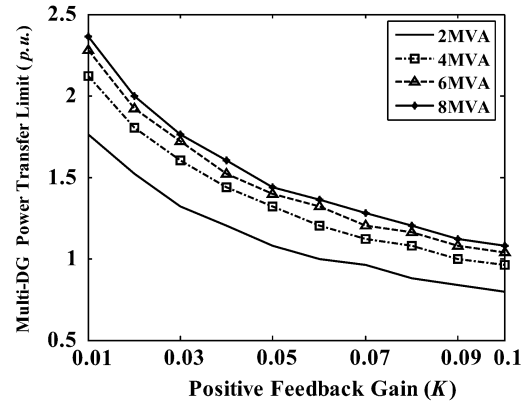


Fig. 9. Impact of substation capacitor on the multi-DG $P - K$ curve.

itor compensates the reactive power consumed by the loads and improves the voltage profile along the feeder, leading to an improvement on the small-signal stability.



(a) Multi-DG power transfer limit for different substation transformer capacity.



(b) Multi-DG power transfer limit for different load transformer capacity.

Fig. 10. Impact of substation and load transformers on the multi-DG $P - K$ curve.

D. Substation and Load Transformers

An increase in the capacity of the substation step-down transformer can also increase the multi-DG penetration limit. The comparative results are shown in Fig. 10(a) where the substation transformer capacity is changed from 10 to 40 MVA. A direct explanation for this outcome is that a high capacity transformer strengthens the connection between the feeder and the transmission system, which leads to an increase in the stability margin. Consequently, the DGs can deliver more power to the distribution system. Similarly, an increase in the capacity of the load transformers can also help to increase the multi-DG penetration level, which is shown in Fig. 10(b). In this case, the connection between the local DG system and the feeder will be made stronger with a high capacity transformer.

E. Feeder Length

Feeder length is another factor affecting the multi-DG penetration level. In Fig. 11, the distance between every two DGs is varied to obtain different $P - K$ curves. It is seen that a long feeder will limit the DG penetration level. This observation is understandable since the feeder impedance becomes larger as

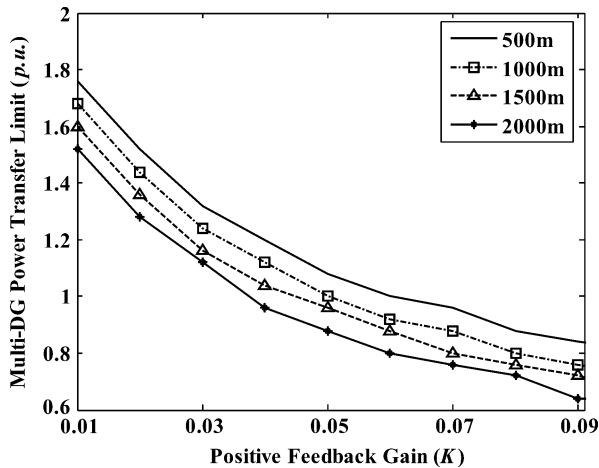


Fig. 11. Impact of feeder length on the multi-DG $P - K$ curve.

the length is increased. The high feeder impedance reduces the power transfer capability of the feeder.

V. INTERACTIONS OF MULTIPLE DGs

The interactions among multiple DGs due to their resident anti-islanding protection are investigated in this section. Fig. 12 shows the interactions for the cases where only DG1 and DG4 are connected to the distribution system feeder. Fig. 12(a) exhibits the variation of the DG1 $P - K$ curve when DG4 output power is fixed at 0.2 p.u., however, its positive feedback gain K_4 is increased from 0.01 to 0.1. From this figure, one can see that the power transfer limit of DG1 decreases due to the increase of positive feedback gain K_4 of DG4. Therefore, one can conclude that the small-signal stability of a single DG equipped with the positive feedback anti-islanding control will be affected by the positive feedback anti-islanding control of another DG installed in the same feeder. Fig. 12(b) exhibits the variation of the DG1 $P - K$ curve when the DG4 output power is changed from 0.1 p.u. to 0.2 p.u. The positive feedback gain of DG4 is set as 0.1 for the two scenarios. It can be observed that the DG1 power transfer limit is reduced when the DG4 output power is increased.

The relationship between the interactions and the number of DGs connected to the feeder is shown in Fig. 13. Fig. 13(a) displays the $P - K$ curves of DG1 for different number of DGs. The curve is highest when only one DG (DG4) is connected and the lowest when three DGs (DG2, DG3, and DG4) are connected. Fig. 13(b) investigates the impact of DG numbers on the $P - K$ curve of DG4. Similarly, the DG4 power transfer limit is reduced with the increase in the DG number. Thus, based on the results in Fig. 13, one can see that the small-signal stability of a single DG equipped with the positive feedback anti-islanding control will be affected by the number of DGs existing in the distribution system no matter if the single DG is close to the substation or at the end of the feeder.

Different distances between two DGs will also change the DG interactions. In Fig. 14(a), the impact of DG4 and DG2 on the DG1 $P - K$ curve is compared. It is known DG4 is electrically farther from DG1 than DG2 is. First, only DG1 and DG4 are connected to the feeder. The $P - K$ curve of DG1 is determined by fixing DG4 output power and its positive feedback

gain. Then only DG1 and DG2 are connected to the feeder and another DG1 $P - K$ curve is obtained by setting P_2 and K_2 constant. The comparison of the two curves shows that DG1 is more vulnerable to DG4. However, a different phenomenon is observed if the impact of DG1 and DG3 on the DG4 $P - K$ curve is compared. It can be seen from Fig. 14(b) that DG3 contributes more instability influence on DG4. That is to say that the DG farther from the substation will have a greater impact on another DG's power transfer limit compared with the DG nearby the substation.

From Fig. 14, one can also draw the conclusion that the closer a generator is to the substation, the lower its interaction with other DGs. This is further demonstrated by Fig. 15 where two cases are compared. In the first case, DG1, DG2 and DG4 are installed in the distribution system. The output power and positive feedback gains of DG1 and DG4 are fixed to obtain the $P - K$ curve of DG2. Correspondingly, the $P - K$ curve of DG3 is obtained in the second case when DG1, DG3, and DG4 are installed. It can be seen from this figure that DG2 has a higher output power limit than that of DG3.

In summary, when a group of inverter-based DGs exist in a given distribution system the small-signal stability of each single generator will be affected by the dynamic controls of other DGs. The interaction between the single generator and the multiple DGs is strong if the DGs have high values of the positive feedback gain for their anti-islanding protection schemes. Also, the interaction is greatly related to the topology of the DG distribution. A generator far away from the substation is easier to lose its stability due to the impact of other DGs.

VI. MULTI-DG STABILITY AND ISLANDING DETECTION TIME

From the stability analysis of the multi-DG system, one knows that the positive feedback gains of the DGs cannot be too strong or they could cause instability even during grid-connected operation. However, for the test system shown in Fig. 4 if the positive feedback gains are low the islanding will not be detected in a timely fashion when the circuit breaker at the substation is open. According to IEEE Std. 1547 [1], all the DG units should be disconnected from the network when an unintentional island is detected. Failure to trip DG units under the unintentional island conditions may cause a number of problems for DG units and the connected loads [11]. Fig. 16 displays the DG2 terminal frequency changes subsequent to the islanding which occurs at 8 s. Three different gain scenarios are compared for the same generation-load level. The results are obtained from electromagnetic transient simulations. In the first scenario, all the positive feedback gains are 0.01. Obviously, the islanding phenomenon can be detected fast under this situation as the islanded DG system loses its stability after the islanding occurrence. While in the second scenario with $K_1 = 0$, $K_2 = K_3 = K_4 = 0.01$, the DGs will not be tripped as the aggregate positive feedback anti-islanding control of the DGs is not strong enough to destabilize the islanded DG system, because the steady-state frequency of the island is within the trip limits of the frequency relays due to the power balance in the island. In the third scenario ($K_1 = 0.05$, $K_2 = K_3 = K_4 = 0$), the DG system becomes unstable after the islanding, however, only DG1 contributes to the destabilizing force, and the system behavior is quite different from the first scenario.

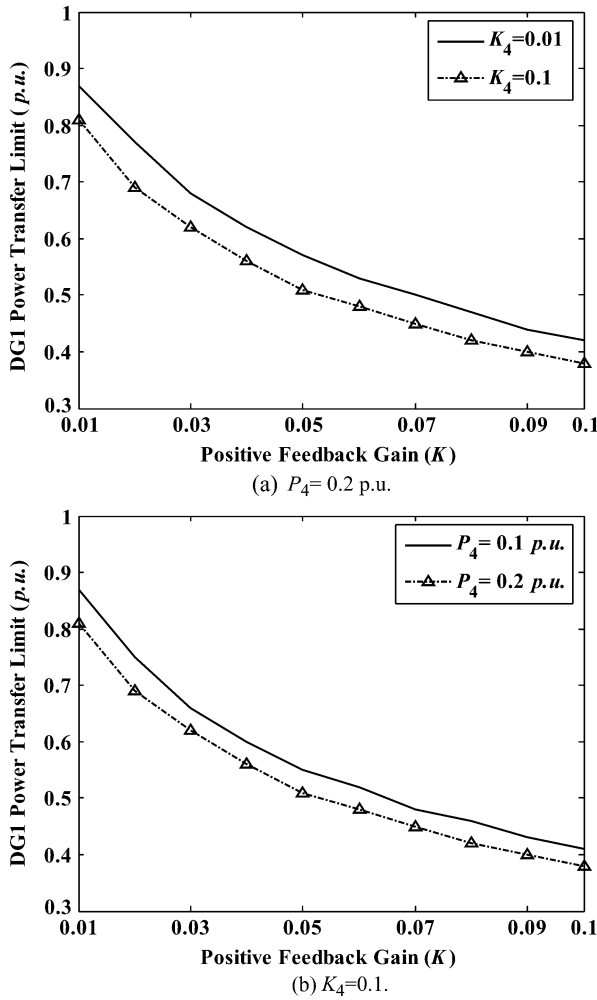


Fig. 12. Interaction between DG4 and DG1.

Thus, there are different combinations of the positive feedback gain settings for the multiple DG units to detect islanding. The choice could be only one or a few generators are equipped with high positive feedback gain while the others are not protected by the positive feedback control or every generator has moderate positive feedback gain. Although these combinations can all destabilize the islanded DG system ultimately, their islanding detection performance is different. For example, in Fig. 16 the third scenario has a shorter islanding detection time than the second scenario. Furthermore, the impact of the anti-islanding control on the grid-connected DG system stability also depends on how the positive feedback gains are distributed among the DG units. Based on these results, there is a need to determine which option leads to a low negative impact on the DGs stability without reducing the islanding detection capability.

The DG power transfer limit versus islanding detection curve ($P-t$ curve) is utilized to quantify the above conflict. This curve is obtained by combining the $P-K$ curve and the islanding detection time versus positive feedback gain curve ($t-K$ curve) of the multi-DG system. A $t-K$ curve is plotted by changing the positive feedback gain value to get the corresponding islanding detection time through electromagnetic transient simulations. The DG output power is fixed during this process.

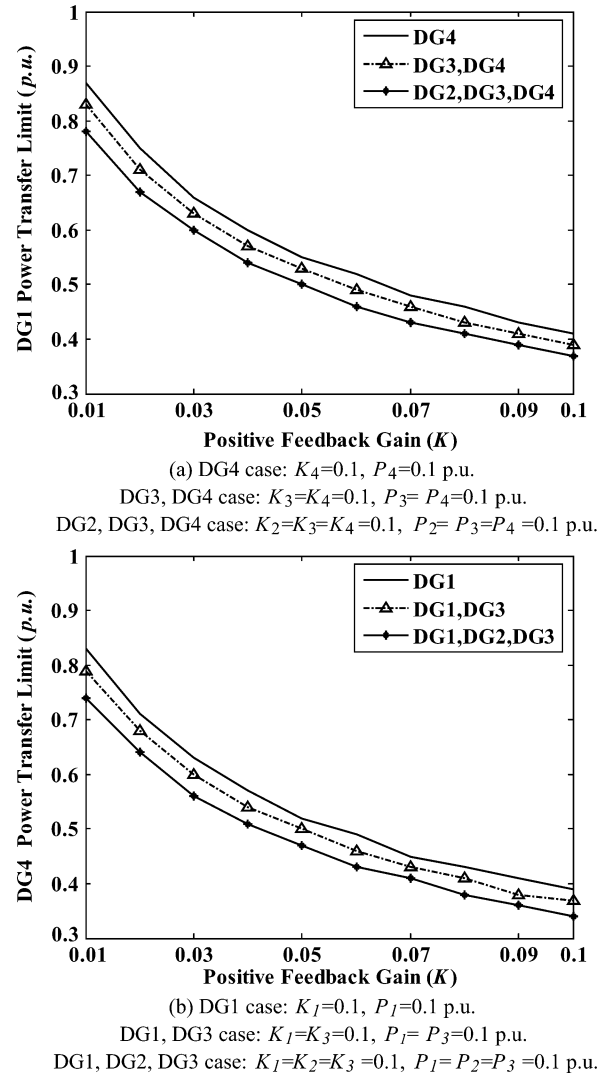
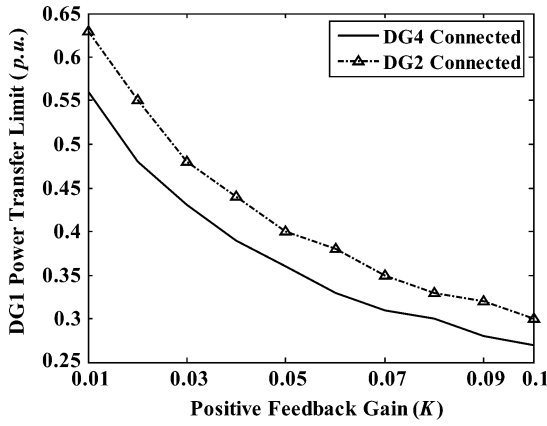


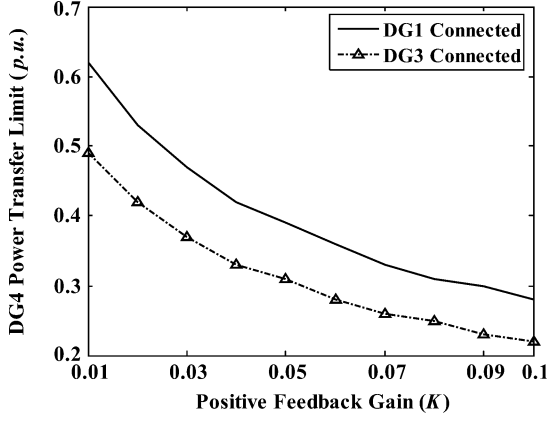
Fig. 13. Effect of DG number on the DG interactions.

Fig. 17 shows the $t-K$ curves of DG1–DG4 for the test system. The output power of all the inverters is 0.185 p.u. for these curves. In the DG1 curve case, K_1 is varied from 0.011 to 0.03 and $K_2 - K_4$ are kept as 0.01. The other three curves are drawn in the same way by increasing one positive feedback gain while fixing the others. It is interesting to note that the curves are almost the same. This phenomenon indicates the DG location has little impact on the islanding detection time. Fig. 18 reveals the $P-K$ curves related to the above four $t-K$ curves, respectively. The “DG1 $P-K$ curve” is obtained by fixing the output power and positive feedback gains of DG2–DG4 and calculating the DG1 power transfer limit for each changing K_1 . The other $P-K$ curves are plotted similarly by varying the parameters of only one inverter. Fig. 19 combines the $t-K$ curves and $P-K$ curves into the $P-t$ curves. From the $P-t$ curves, it is clear to see that the DG system has the highest power transfer limit for the DG1 curve case if the islanding detection time is required to be the same for the four cases.

The interaction among the multiple DG units in the $P-t$ curve study is illustrated in Fig. 20 where the DG1 curve case shown in Fig. 19 is compared with a new case which has $K_2 = 0.02$. Only K_2 is different in these two cases. From Fig. 20 one



(a) DG4 case: $K_4=0.2, P_4=0.2$ p.u. ; DG2 case: $K_2=0.2, P_2=0.2$ p.u.



(b) DG1 case: $K_1=0.2, P_1=0.2$ p.u. ; DG3 case: $K_3=0.2, P_3=0.2$ p.u.

Fig. 14. Effect of distance on the DG interactions.

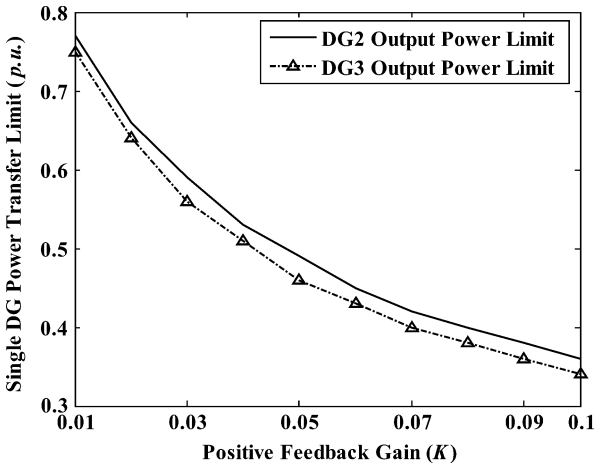


Fig. 15. Comparison of the interactions of DG2 with DG1 and DG4 and of DG3 with DG1 and DG4 ($K_1 = K_4 = 0.1, P_1 = P_4 = 0.1$ p.u.).

can see if the same DG1 power transfer limit is required by the two cases; the case with $K_2 = 0.02$ (point A) has the shorter islanding detection time than that of the case with $K_2 = 0.01$ (point B). In fact, point C has the same K_1 value with point A, while K_2 is different for these two points. The behavior in Fig. 20 can be explained as follows: assume $K_1 = K_2 = K_3 = K_4 = 0.01$ and that we want to shorten the DG system islanding detection time. Should we increase K_1 to 0.017 and keep other

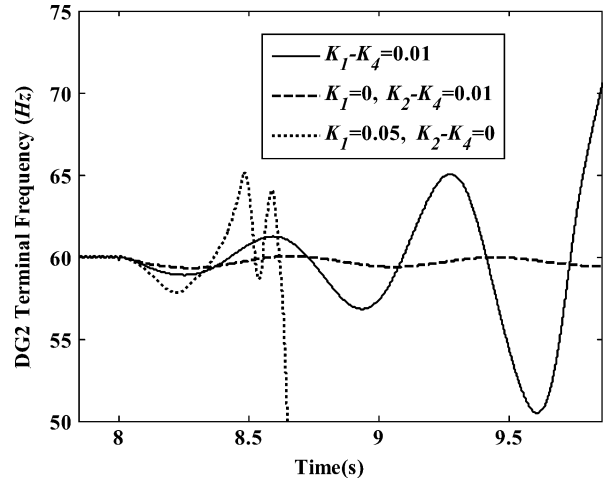


Fig. 16. DG2 terminal frequency of the islanded DG system.

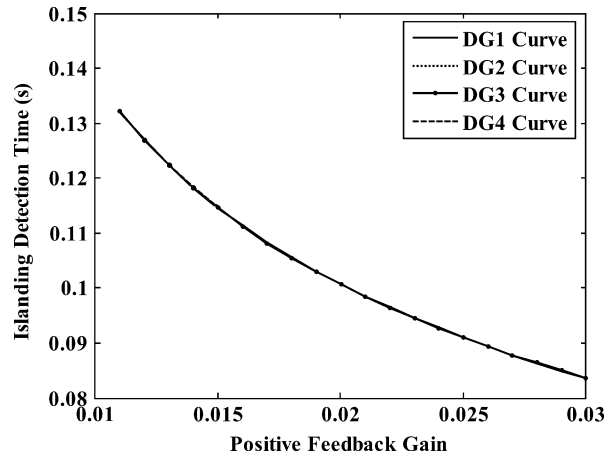


Fig. 17. $t - K$ curves of DG1–DG4.

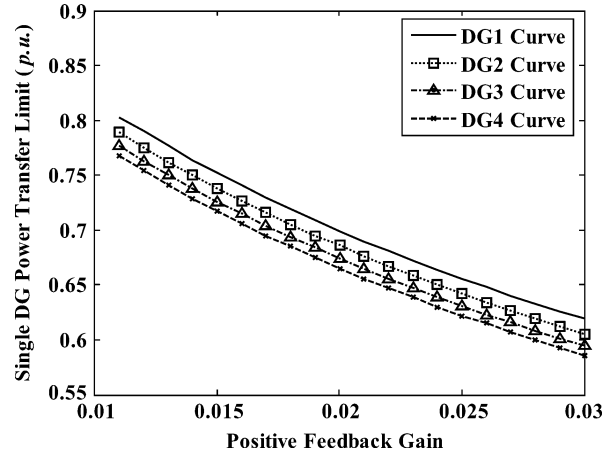
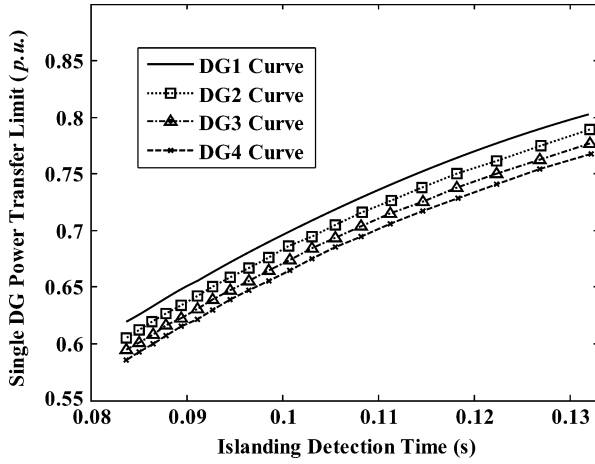
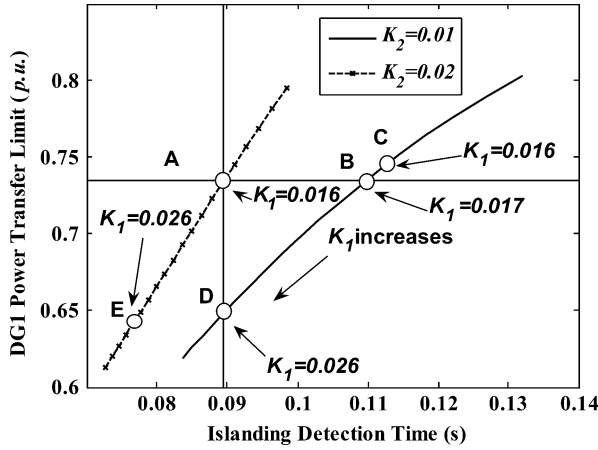


Fig. 18. $P - K$ curves of DG1–DG4.

gains unchanged or increase K_1 to 0.016 and K_2 to 0.02? Actually, these two methods have the same impact on the DG1 power transfer limit. However, the latter method has a smaller islanding detection time. Similarly, if the same islanding detection time is required by the two cases point A should be used instead of point D as the DG1 power transfer limit is larger for point A. Thus, by using this curve, one can find a trade-off solution between

Fig. 19. $P - t$ curves of DG1-DG4.Fig. 20. Impact of K_2 on the DG1 $P - t$ curve.

the maximum power transfer limit and islanding detection capability.

VII. CONCLUSION

This paper presented a small-signal stability analysis of the multi-DG system with the positive feedback anti-islanding scheme. The paper introduced the multi-DG power transfer limit versus positive feedback gain curve as an index to determine and analyze the stability of multi-DG system. By using this curve, an extensive sensitivity study was conducted. According to the sensitivity analysis results, it was concluded that the maximum multi-DG penetration level in an existing distribution system is limited by the destabilizing effect of the positive feedback anti-islanding control. The relationship between the multi-DG system stability and the positive feedback anti-islanding protection capability was also quantified. The tools developed in this paper are useful for analysis and design of the inverter-based DGs with the positive feedback anti-islanding protection.

APPENDIX A

The model of the multi-DG system is shown in Fig. 21, where \mathbf{n} is the number of DGs and \mathbf{m} is the number of loads. The model is composed of the DG block, the network and loads block and

the interface block. In the DG block each inverter-based distributed generator model is expressed in its own $d - q$ reference frame [10] where the DG terminal voltage phase angle is set as zero. The small-signal model equations of DGs are expressed as follows:

$$p\Delta\mathbf{u}_d = \mathbf{k}_{pi}p(\Delta\mathbf{i}_{dref}^* - \Delta\mathbf{i}_d) + \mathbf{k}_{ii}(\Delta\mathbf{i}_{dref}^* - \Delta\mathbf{i}_d) \quad (3)$$

$$p\Delta\mathbf{u}_q = \mathbf{k}_{pi}p(\Delta\mathbf{i}_{qref}^* - \Delta\mathbf{i}_q) + \mathbf{k}_{ii}(\Delta\mathbf{i}_{qref}^* - \Delta\mathbf{i}_q) \quad (4)$$

$$\Delta\mathbf{u}_d = \mathbf{L}_s p\Delta\mathbf{i}_d \quad (5)$$

$$\Delta\mathbf{u}_q = \mathbf{L}_s p\Delta\mathbf{i}_q \quad (6)$$

$$p\Delta\mathbf{i}_{dref} = -\mathbf{k}_{pp}p\Delta\mathbf{P} - \mathbf{k}_{ip}\Delta\mathbf{P} \quad (7)$$

$$p\Delta\mathbf{i}_{qref} = \mathbf{k}_{pp}p\Delta\mathbf{Q} - \mathbf{k}_{ip}\Delta\mathbf{Q} \quad (8)$$

$$\Delta\mathbf{P} = \mathbf{v}_{d0}\Delta\mathbf{i}_d + \mathbf{i}_{d0}\Delta\mathbf{v}_d + \mathbf{v}_{q0}\Delta\mathbf{i}_q + \mathbf{i}_{q0}\Delta\mathbf{v}_q \quad (9)$$

$$\Delta\mathbf{Q} = \mathbf{v}_{d0}\Delta\mathbf{i}_q + \mathbf{i}_{q0}\Delta\mathbf{v}_d - \mathbf{v}_{q0}\Delta\mathbf{i}_d - \mathbf{i}_{d0}\Delta\mathbf{v}_q \quad (10)$$

$$p\Delta\boldsymbol{\omega} = \mathbf{k}_p p\Delta\mathbf{v}_q + \mathbf{k}_i\Delta\mathbf{v}_q \quad (11)$$

$$p\Delta\boldsymbol{\delta} = \Delta\boldsymbol{\omega} \quad (12)$$

$$\Delta\boldsymbol{\theta}_f = \frac{\pi}{2}\mathbf{K}\Delta\boldsymbol{\omega} \quad (13)$$

$$\Delta\mathbf{i}_{dref}^* = \cos\boldsymbol{\theta}_{f0}\Delta\mathbf{i}_{dref} - \sin\boldsymbol{\theta}_{f0}\Delta\mathbf{i}_{qref} - \mathbf{i}_{q0}\Delta\boldsymbol{\theta}_f \quad (14)$$

$$\Delta\mathbf{i}_{qref}^* = \sin\boldsymbol{\theta}_{f0}\Delta\mathbf{i}_{dref} + \cos\boldsymbol{\theta}_{f0}\Delta\mathbf{i}_{qref} + \mathbf{i}_{d0}\Delta\boldsymbol{\theta}_f \quad (15)$$

where the variables in the model are vectors and each vector is composed of \mathbf{n} elements which are related to the variables of the single DG model. For example, the voltage vectors $\Delta\mathbf{u}_d$ and $\Delta\mathbf{u}_q$ have the following definitions:

$$\Delta\mathbf{u}_d = [\Delta u_{d1}, \Delta u_{d2}, \dots, \Delta u_{dn}]^T \quad (16)$$

$$\Delta\mathbf{u}_q = [\Delta u_{q1}, \Delta u_{q2}, \dots, \Delta u_{qn}]^T. \quad (17)$$

Also, the diagonal matrices \mathbf{v}_{d0} , \mathbf{v}_{q0} , \mathbf{i}_{d0} , \mathbf{i}_{q0} , $\cos\boldsymbol{\theta}_{f0}$, $\sin\boldsymbol{\theta}_{f0}$, \mathbf{k}_{pi} , \mathbf{k}_{ii} , \mathbf{k}_{pp} , \mathbf{k}_{ip} , \mathbf{k}_i , \mathbf{k}_p , \mathbf{L}_s , and \mathbf{K} have the following definitions: $\mathbf{v}_{d0} = \text{diag}\{v_{d0j}\}$, $\mathbf{v}_{q0} = \text{diag}\{v_{q0j}\}$ (inverter terminal voltages), $\mathbf{i}_{d0} = \text{diag}\{i_{d0j}\}$, $\mathbf{i}_{q0} = \text{diag}\{i_{q0j}\}$ (inverter output currents), $\cos\boldsymbol{\theta}_{f0} = \text{diag}\{\cos\theta_{f0j}\}$, $\sin\boldsymbol{\theta}_{f0} = \text{diag}\{\sin\theta_{f0j}\}$ (SFS transformation angles), $\mathbf{k}_{pi} = \text{diag}\{k_{pij}\}$, $\mathbf{k}_{ii} = \text{diag}\{k_{iij}\}$ (inverter power regulator constants), $\mathbf{k}_{pp} = \text{diag}\{k_{ppj}\}$, $\mathbf{k}_{ip} = \text{diag}\{k_{ipj}\}$ (inverter current regulator constants), $\mathbf{k}_i = \text{diag}\{k_{ij}\}$, $\mathbf{k}_p = \text{diag}\{k_{pj}\}$ (inverter phase-locked loop controller constants), $\mathbf{L}_s = \text{diag}\{L_{sj}\}$ (inverter output filter inductances), and $\mathbf{K} = \text{diag}\{K_j\}$ (positive feedback gains) with $j = 1, 2, \dots, n$. The superscript T indicates the transpose of vector and the sub-superscript 0 denotes the steady-state values of the DG variables. The small-signal model equations of the network and loads are expressed in the common reference frame ($x - y$ frame) and can be written as

$$\begin{bmatrix} \Delta\mathbf{i}_x \\ \Delta\mathbf{i}_y \end{bmatrix} = \begin{bmatrix} \mathbf{G} & -\mathbf{B} \\ \mathbf{B} & \mathbf{G} \end{bmatrix} \begin{bmatrix} \Delta\mathbf{v}_x \\ \Delta\mathbf{v}_y \end{bmatrix} \quad (18)$$

where the matrices \mathbf{G} and \mathbf{B} are acquired from the network system admittance matrix and

$$\Delta\mathbf{v}_x = [\Delta v_{x1}, \Delta v_{x2}, \dots, \Delta v_{xn}]^T \quad (19)$$

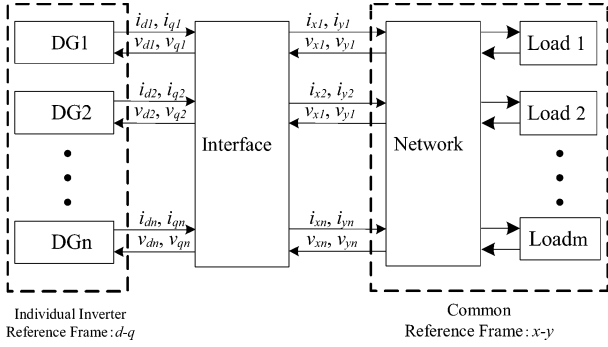


Fig. 21. Structure of the multi-DG system model.

$$\Delta \mathbf{v}_y = [\Delta v_{y1}, \Delta v_{y2}, \dots, \Delta v_{yn}]^T \quad (20)$$

$$\Delta \mathbf{i}_x = [\Delta i_{x1}, \Delta i_{x2}, \dots, \Delta i_{xn}]^T \quad (21)$$

$$\Delta \mathbf{i}_y = [\Delta i_{y1}, \Delta i_{y2}, \dots, \Delta i_{yn}]^T. \quad (22)$$

The interface equations are

$$\Delta \mathbf{v}_d = \mathbf{C}_0 \Delta \mathbf{v}_x - \mathbf{v}_{x0} \mathbf{S}_0 \Delta \delta + \mathbf{S}_0 \Delta \mathbf{v}_y + \mathbf{v}_{y0} \mathbf{C}_0 \Delta \delta \quad (23)$$

$$\Delta \mathbf{v}_q = \mathbf{S}_0 \Delta \mathbf{v}_x - \mathbf{v}_{x0} \mathbf{C}_0 \Delta \delta + \mathbf{C}_0 \Delta \mathbf{v}_y + \mathbf{v}_{y0} \mathbf{S}_0 \Delta \delta \quad (24)$$

$$\Delta \mathbf{i}_x = \mathbf{C}_0 \Delta \mathbf{i}_d - \mathbf{i}_{d0} \mathbf{S}_0 \Delta \delta - \mathbf{S}_0 \Delta \mathbf{i}_q - \mathbf{i}_{q0} \mathbf{C}_0 \Delta \delta \quad (25)$$

$$\Delta \mathbf{i}_y = \mathbf{S}_0 \Delta \mathbf{i}_d + \mathbf{i}_{d0} \mathbf{C}_0 \Delta \delta + \mathbf{C}_0 \Delta \mathbf{i}_q - \mathbf{i}_{q0} \mathbf{S}_0 \Delta \delta \quad (26)$$

where δ_i is the individual inverter terminal voltage phase angle when it is seen from the $x - y$ frame and the diagonal matrices \mathbf{C}_0 and \mathbf{S}_0 are defined as $\mathbf{C}_0 = \text{diag}\{\cos \delta_{i0}\}$ and $\mathbf{S}_0 = \text{diag}\{\sin \delta_{i0}\}$.

APPENDIX B

In this appendix, some simulation studies are conducted to validate and justify the small-signal model used in this paper. In order to carry out these studies, the Canadian urban benchmark distribution system shown in Fig. 4 is used.

Dynamic Response for a Reference Step: In this subsection, the small-signal model is verified in time domain by comparing the dynamic response for a reference step obtained from an electromagnetic transient-type model, set up in Matlab/Simulink, and from the small-signal model. Fig. 22 shows the result. The network parameter settings are listed in Table II and the DGs parameter settings are listed in Table III. The local loads of the DGs are all with the capacity of 2 MVA and the power factor of 0.95. The figure presents the dynamic behavior of the active power injected by DG1 when its reference power P_{ref1} is stepped from 0.1 p.u. to 0.11 p.u. at $t = 0.75$ s. The DG1 reactive power Q_{ref1} is kept in zero. The active power and the reactive power references for the other DGs are 0.1 p.u. and 0 p.u., respectively. The verification result shows that the output power response of the small-signal model is very close to the result from the electromagnetic transients program (EMTP) simulation. Different system parameters and input references were tested for all the DGs. The comparison results, which are not shown here, also indicate the same phenomenon. This demonstrates the accuracy of the small-signal model.

Stability Limit: In this subsection, the small-disturbance stability limit obtained by using the modal anal-

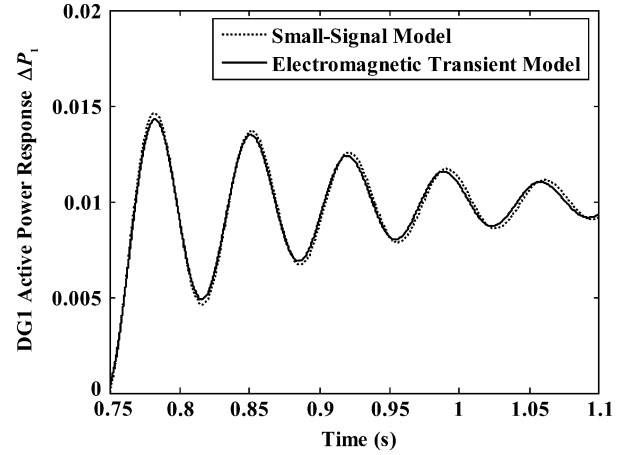


Fig. 22. Model verification: DG1 active power response for a reference step-time domain response.

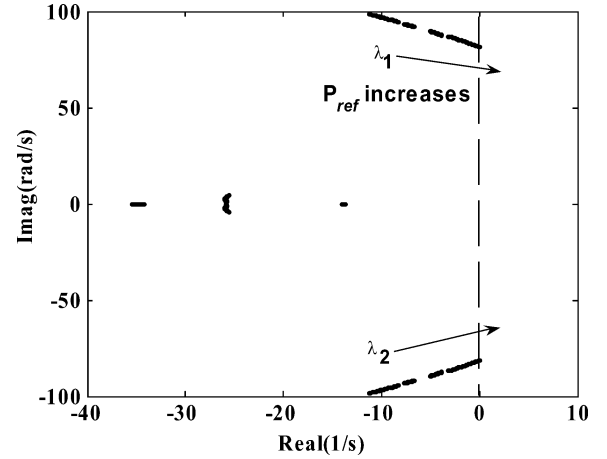


Fig. 23. Model verification: root loci of the multiple DG system.

ysis and the small-signal model is compared with the stability limit obtained by using the electromagnetic transients-typed model. The system parameters are the same with those in Tables II and III. The real power reference vector $\mathbf{P}_{ref} = [P_{ref1}, P_{ref2}, P_{ref3}, P_{ref4}]^T$ is gradually increased from $[0.2, 0.2, 0.2, 0.2]^T$ p.u. to $[0.45, 0.45, 0.45, 0.45]^T$ p.u. to observe the root loci of the small-signal model. The step of the change is the same for each DG. The reactive power reference vector $\mathbf{Q}_{ref} = [Q_{ref1}, Q_{ref1}, Q_{ref1}, Q_{ref1}]^T$ is set as zero. Fig. 23 displays the root loci of the multiple DG system when the vector \mathbf{P}_{ref} is varied. One can see that a pair of conjugate eigenvalues moves from the left half-plane to the right half-plane when \mathbf{P}_{ref} is increased. It is known that the DG system will lose its small-signal stability once there are eigenvalues with positive real parts. As a result, at this point there is a value of \mathbf{P}_{ref} related to the system stability limit. The eigenvalue analysis of the developed small-signal model indicates that the stability limit of the DG system \mathbf{P}_{ref} is equal to $[0.45, 0.45, 0.45, 0.45]^T$ p.u. Fig. 24 shows the stability limit obtained by the time domain model. The vector \mathbf{P}_{ref} is stepped from $[0.2, 0.2, 0.2, 0.2]^T$ p.u. to $[0.4, 0.4, 0.4, 0.4]^T$ p.u. at $t = 1.5$ s. After this instant, the DG1 output power P_1 begins to oscillate and after a decaying time, the DG

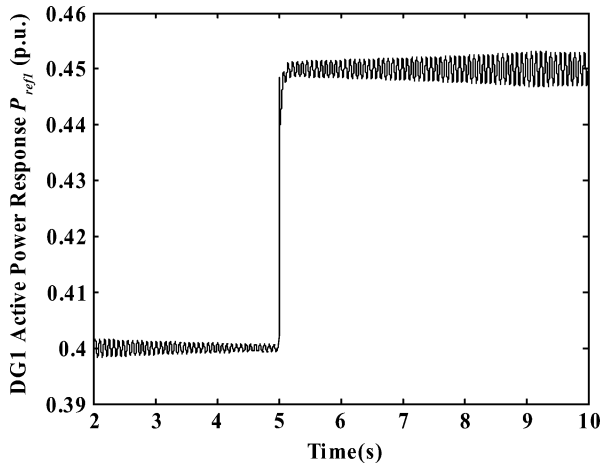


Fig. 24. Model verification: DG1 active power response—stability limit.

TABLE II
DISTRIBUTION SYSTEM PARAMETERS

| Parameters | Value |
|-------------|------------------------------|
| S_{base} | 10 (MVA) |
| V_{base1} | $120\sqrt{2}/\sqrt{3}$ (kV) |
| V_{base2} | $12.5\sqrt{2}/\sqrt{3}$ (kV) |
| V_{base3} | $208\sqrt{2}/\sqrt{3}$ (V) |
| R_s | 0 (p.u.) |
| X_s | 0 (p.u.) |
| R_T | 0 (p.u.) |
| X_T | 0.1 (p.u.) |
| R_f | 0.0029 (p.u.) |
| X_f | 0.0041 (p.u.) |
| R_l | 0 (p.u.) |
| X_l | 0.2 (p.u.) |

TABLE III
INVERTER PARAMETERS

| Parameters | Value |
|--|------------|
| K_{pp} | 2.5 |
| K_{ip} | 100 |
| K_{pi} | 2.5 |
| K_{ii} | 500 |
| L_s | 1 (mH) |
| K_p | 50 |
| K_i | 500 |
| K_1, K_2, K_3, K_4 | 0.01 |
| $cf_{01}, cf_{02}, cf_{03}, cf_{04}$ | 0 |
| $P_{ref1}, P_{ref2}, P_{ref3}, P_{ref4}$ | 0.1 (p.u.) |
| $Q_{ref1}, Q_{ref2}, Q_{ref3}, Q_{ref4}$ | 0 (p.u.) |

reaches a new steady-state operating point. The power reference P_{ref} is then stepped from $[0.4, 0.4, 0.4, 0.4]^T$ p.u. to $[0.45, 0.45, 0.45, 0.45]^T$ p.u. at $t = 5$ s and the DG system begins to oscillate at this power level and becomes unstable, which meets the limit obtained by modal analysis.

APPENDIX C

Table II lists the distribution system parameters, and Table III lists the inverter parameters.

REFERENCES

- [1] *Standard for Interconnecting Distributed Resources With Electric Power Systems*, IEEE Std. 1547-2003, 2003.
- [2] M. E. Ropp, M. Begovic, and A. Rohatgi, "Analysis and performance assessment of the active frequency drift method of islanding prevention," *IEEE Trans. Energy Convers.*, vol. 14, no. 3, pp. 810–816, Sep. 1999.
- [3] J. Stevens, R. Bonn, J. Ginn, S. Gonzalez, and G. Kern, Development and Testing of an Approach to Anti-Islanding in Utility-Interconnected Photovoltaic Systems, Sandia Report SAND200-1939, 2000. [Online]. Available: <http://www.sandia.gov/pv/docs/PDF/0800steve.pdf>.
- [4] Z. Ye, R. Walling, L. Garces, R. Zhou, L. Li, and T. Wang, Study and Development of Anti-Islanding Control for Grid-Connected Inverters National Renewable Energy Laboratory, , 2004, Tech. Rep. NREL/SR-560-36243.
- [5] X. Wang and W. Freitas, "Impact of positive feedback anti-islanding methods on small-signal stability of inverter-based distributed generation," *IEEE Trans. Energy Convers.*, vol. 23, no. 3, pp. 923–931, Sep. 2008.
- [6] S. J. Ranade, R. P. Nadipuram, S. Omick, and L. F. Kazda, "A study of islanding in utility-connected residential photovoltaic systems—Part I: Models and analytical methods," *IEEE Trans. Energy Convers.*, vol. 4, no. 3, pp. 436–445, Sep. 1989.
- [7] S. J. Ranade, R. P. Nadipuram, S. Omick, and L. F. Kazda, "A study of islanding in utility-connected residential photovoltaic systems—part II: Case studies," *IEEE Trans. Energy Convers.*, vol. 4, no. 3, pp. 446–452, Sep. 1989.
- [8] V. John, Z. Ye, and A. Kolwalkar, "Investigation of anti-islanding protection of power converter based distributed generators using frequency domain analysis," *IEEE Trans. Power Electron.*, vol. 19, no. 5, pp. 1177–1183, Sep. 2004.
- [9] E. P. Dick and A. Narang, Canadian Urban Benchmark Distribution Systems, CANMET Energy Technology Centre–Varennes, Nature Resources Canada, 2005. [Online]. Available: <http://cetc-varennes.nrcan.gc.ca/fichier.php/codectec/En/2005-121/2005-121e.pdf>.
- [10] P. Kundur, *Power System Stability and Control*. New York: McGraw-Hill, 1994.
- [11] W. Bower and M. E. Ropp, *Evaluation of Islanding Detection Methods for Photovoltaic Utility-Interactive Power Systems*. International Energy Agency: Task V IEA-VPVS T5-09, 2002.

Xiaoyu Wang (S'03–M'08) received the B.Sc. degree and the M.Sc. degree in electrical engineering from Tsinghua University, Beijing, China, in 2000 and 2003, respectively, and the Ph.D. degree in the Department of Electrical and Computer Engineering at the University of Alberta, Edmonton, AB, Canada, in 2008.

Currently, he is an Assistant Researcher at Tsinghua University. His research interests include distributed generation and power system stability.

Walmir Freitas (M'02) received the Ph.D. degree in electrical engineering from the State University of Campinas, Campinas, Brazil, in 2001.

Currently, he is an Associate Professor at the University of Campinas. His research interests are distribution systems, protection systems, and distributed generation.

Venkata Dinavahi (M'00) received the Ph.D. degree in electrical and computer engineering from the University of Toronto, Toronto, ON, Canada, in 2000.

Presently, he is an Associate Professor at the University of Alberta, Edmonton, AB, Canada. His research interests include electromagnetic transient analysis, power electronics, real-time simulation, and control.

Wilsun Xu (M'90–SM'95–F'05) received the Ph.D. from the University of British Columbia, Vancouver, BC, Canada, in 1989.

From 1989 to 1996, he was with B.C. Hydro as an Electrical Engineer. He joined the University of Alberta, Edmonton, AB, Canada, in September 1996 and is presently a Professor of electrical engineering. His research interests are power quality and distributed generation.